Plant, Cell and Environment (2007) **30**, 1223–1239 doi: 10.1111/j.1365-3040.2007.01703.x

Diurnal, seasonal and interannual variability of carbon isotope discrimination at the canopy level in response to environmental factors in a boreal forest ecosystem

BAOZHANG CHEN* & JING M. CHEN

Department of Geography and Program in Planning, University of Toronto, Ontario, Canada

ABSTRACT

Accurate estimation of temporal and spatial variations in photosynthetic discrimination of ^{13}C is critical to carbon cycle research. In this study, a combined ecosystem–boundary layer isotope model, which was satisfactorily validated against intensive campaign data, was used to explore the temporal variability of carbon discrimination in response to environmental driving factors in a boreal ecosystem in the vicinity of Fraserdale Tower, Ontario, Canada (49°52′30″N, 81°34′12″W). A 14 year (1990–1996 and 1998–2004) hourly CO_2 concentration and meteorological record measured on this tower was used for this purpose. The 14 year mean yearly diurnal amplitude of canopy-level discrimination Δ_{canopy} was computed to be 2.8 ± 0.5‰, and the overall diurnal cycle showed that the greatest Δ_{canopy} values occurred at dawn and dusk, while the minima generally appeared in mid-afternoon. The average annual Δ_{canopy} varied from 18.3 to 19.7‰ with the 14 year average of 19 ± 0.4‰. The overall seasonality of Δ_{canopy} showed a gradually increasing trend from leaf emergence in May–September and with a slight decrease at the end of the growing season in October. Δ_{canopy} was negatively correlated to vapour pressure deficit and air temperature across hourly to decadal timescales. A strong climatic control on stomatal regulation of ecosystem isotope discrimination was found in this study.

Key-words: BEPS-EASS; biosphere–atmosphere interaction; carbon isotopes; isotope model; planetary boundary layer.

INTRODUCTION

Concerns over the increasing concentration of atmospheric CO_2 and its subsequent effects on global warming have led to use of new techniques to resolve the global carbon budget (Canadell *et al.* 2000). One of these techniques is isotopic mass balance models (Tans 1980; Ciais *et al.* 1995a; Fung *et al.* 1997; Battle *et al.* 2000; Randerson *et al.* 2002b). This technique capitalizes on the seasonal oscillations in $\delta^{13}C$ of atmospheric CO_2 that are mainly driven by discrimination against ^{13}C by terrestrial ecosystems. The atmospheric inversion models rely on estimates of photosynthetic discrimination (Δ) and the ^{13}C of ecosystem-respired CO_2 (Tans, Berry & Keeling 1993; Fung *et al.* 1997) to assess variations in the magnitude of the terrestrial carbon sink. Canopy level or whole ecosystem Δ can be determined from the isotopic signature of CO_2 in the convective boundary layer (CBL), which includes the effects of respiration, photosynthesis and turbulent transport (Lloyd *et al.* 1996; Chen *et al.* 2006a).

Previous studies have assumed that carbon isotope discrimination by terrestrial ecosystems remains constant from year to year (Randerson *et al.* 2002b). This approximation has been widely employed on many timescales (e.g. Ciais *et al.* 1995b; Joos & Bruno 1998; Trudinger *et al.* 1999; Battle *et al.* 2000; Keeling *et al.* 2001). However, plant Δ against ^{13}C during photosynthesis may vary in seasonal and inter-annual time frames. Observations at the ecosystem scale (e.g. Bowling *et al.* 2002) have indicated that Δ does not remain constant. Inter-annual variability in Δ by nutrient and moisture stresses would be interpreted by inversion models as a shift in the terrestrial and oceanic sinks (Randerson *et al.* 2002b). The variability in Δ will alter the conclusions about the timing and nature of the terrestrial carbon sink (Bowling *et al.* 2002). Fung *et al.* (1997) indicated that a 3‰ overestimation in the global value of discrimination would result in a 20% underestimation in the magnitude of the biospheric sink. Several recent ecosystem studies provide evidence that Δ is highly variable on synoptic through inter-annual timescales (e.g. Kaplan, Prentice & Buchmann 2002; Randerson *et al.* 2002a,b; Suits *et al.* 2005; Aranibar *et al.* 2006). Hence, accurate parameterization of models that predict temporal and spatial variations in Δ is useful for improving the global carbon budget (Randerson *et al.* 2002a).

The biosphere–atmosphere isotopic disequilibrium is strongly controlled by photosynthetic discrimination and the carbon isotope signature of the terrestrial biosphere,

Correspondence: B. Chen. Fax: 604 822 2184; e-mail: baozhang.chen@ubc.ca

*Present address: Biometeorology and Soil Physics Group, Faculty of Land and Food Systems, University of British Columbia, 2357 Main Mall, Vancouver, British Columbia, Canada, V6T 1Z4.

which may change from year to year as vegetation composition and carbon-exchange characteristics respond to climatic variability (McGuire *et al.* 2001). Studies of environmental and biological controls of Δ (e.g. Baldocchi & Bowling 2003; Suits *et al.* 2005; Aranibar *et al.* 2006) have revealed a number of factors that cause discrimination to vary (Farquhar, Ehleringer & Hubick 1989). These include atmospheric humidity, solar radiation, drought stress and plant type, all of which may be expected to respond to inter-annual climate variability.

Most existing approaches to study photosynthetic discrimination are dependent, to some degree, on measurements of $^{13}C/^{12}C$ in the atmosphere. Multiple efforts to measure carbon isotopes at both flux towers and flask stations around the world have been made (e.g. Bowling *et al.* 2003b; Lai *et al.* 2003, 2004; Griffis *et al.* 2004; McManus *et al.* 2005; Schauer *et al.* 2005). Although available isotopic data sets are being accumulated quickly (e.g. Griffis, Baker & Zhang 2005; Lai *et al.* 2005, 2006; Ponton *et al.* 2006; Zhang, Griffis & Baker 2006), isotope measurements are still lacking in comparison to land surface diversity and heterogeneity. This shortage of long-term measurements and of sampling frequency still limits isotopic discrimination studies.

Mechanistic biophysical models that couple micrometeorological and eco-physiological theories have the potential to shed light on how to extend the use of available measurements of stable isotopes of carbon dioxide to global carbon budgeting, because biophysical models have the capacities of simulating isotope discrimination in response to environmental perturbations and can produce information on its diurnal, seasonal and inter-annual dynamics. In this study, a combined ecosystem–boundary layer isotope model [Vertical Diffusion Scheme (VDS)–Boreal Ecosystem Productivity Simulator (BEPS)–Ecosystem Atmosphere Simulation Scheme (EASS)] was used to investigate inter-annual temporal variations in ecosystem-level Δ and to explore the responses of Δ to environmental factors in a boreal ecosystem. This integrated modelling system is designed for inclusion in global models. It has the ability to simulate dynamics of the stable isotope ^{13}C in CO_2, as well as moisture, energy and momentum, between ecosystems and the atmosphere as well as their diffusion processes through planetary boundary layer (PBL). It uses remotely sensed land surface parameters to characterize the surface heterogeneity and is driven by hourly meteorology in the surface layer. It has the following characteristics: (1) it accounts for the influences of the PBL turbulent mixing and entrainment of the air aloft; (2) it scales individual leaf-level Δ up to the whole canopy (Δ_{canopy}) through the separation of sunlit and shaded leaf groups; (3) it has the capacity of exploring the responses of Δ to environmental and physiological driving factors, and (4) it has the potential to investigate how an ecosystem discriminates against ^{13}C at various temporal and spatial scales. This isotope model has also been validated against intensive campaigns (1998–2000) and weekly diurnal sampling data at a boreal forest site (Fraserdale, Canada) (Chen *et al.* 2006a). It has also been used to study dynamics of $\delta^{13}C$ of CO_2 in the PBL and the covariation between the surface isotope flux and atmospheric mixing over a boreal forest region (Chen *et al.* 2006b). In this paper, we report an application of this model to a 14 year series data (1990–1996 and 1998–2004) measured at Fraserdale tower, Ontario, Canada (49°52′30″N, 81°34′12″W), in order to explore inter-annual temporal variations of ecosystem-level Δ in response to environmental factors in a boreal ecosystem.

MATERIALS AND METHODS

Study site

The Fraserdale tower is located southwest of James Bay in northern Ontario, Canada (49°52′29.9″N, 81°34′12.3″W; 210 m above sea level). According to a Landsat Thematic Mapper (TM) image at a 30 m resolution acquired in 1998, the landscape (3600 km^2 around the tower) consisted of 66% of black spruce (*Picea mariana*) and jack pine (*Pinus banksiana*), 20% open land after forest fires and logging, 11% aspen (*Populus tremuloides*) and paper birch (*Betula papyrifera*), and 3% open water. The overstorey vegetation heights around this site ranged from 10 to 15 m. In the prevailing northwest wind direction, the forests were predominantly undisturbed.

The atmospheric CO_2 was continuously monitored at 40 and 20 m heights at the Fraserdale tower. The measurements were made according to the World Meteorological Organization (WMO) (Global Atmospheric Watch) guidelines, with an accuracy of 1×10^{-4} mg g^{-1} (Higuchi *et al.* 2003). The measurements were initiated in February 1990 and continued to November 1996. After an interruption of around 1.5 years (December 1996–May 1998), the measurement programme was restored in June 1998, and continues to the present day. Detailed site description and the measurement programme are found in Higuchi *et al.* (2003) and Chen, Chen & Worthy (2005).

Model description

The VDS–BEPS–EASS isotope model is a one-dimensional integrated ecosystem–boundary layer model, which is based on isotopic mass conservation and energy balance. The model consists of two coupled components: (1) VDS and (2) coupled BEPS–EASS.

The atmospheric transport model (VDS) simulates the transport processes of scalar entities (e.g. CO_2, temperature) from the surface layer through the top of PBL at 30 s time step (Chen *et al.* 2004; Chen, Chen & Worthy 2005). There are different schemes (modules) to treat different situations of the PBL structures [stable boundary layer (SBL) or CBL] (Chen, Chen & Worthy 2005). The criteria that determine which module is applicable are the sign and magnitude of the bulk Richardson number (R_b) in the surface layer and the magnitude of the ratio of the CBL height to the Monin Obukhov length ($|z_h/L|$). VDS has been expanded to simulate diffusion processes of stable carbon isotopic signature of CO_2 as well [(Chen *et al.* 2006a,b; for detail, see Appendix B in the paper by Chen *et al.* (2006a)].

The time step for VDS is 30 s. The influences of the CBL turbulent mixing and entrainment of the air aloft on diffusion and on the estimates of ^{13}C discrimination are also considered in this model.

The land surface model (BEPS–EASS) simulates energy, water and carbon fluxes among the soil, canopy and the atmosphere at a user-defined time step using hourly or half-hourly measured meteorological data (Chen, Chen & Ju 2007; Chen *et al.* 2007). In BEPS–EASS, the soil profile is split into multiple layers (five were used in this study); for each of them, temperature and water content are simulated separately. It has been expanded to include a sub-model to simulate photosynthetic discrimination and net isotope flux at the canopy level (Chen *et al.* 2006a; for detail, see Appendix A of that paper).

BEPS–EASS is a 'two-leaf' carbon isotope canopy model. It has less complexity in formulation than the 'multilayer' model and has the advantage of avoiding shortcomings of the 'big-leaf' canopy model shown by Chen *et al.* (1999). Such a two-leaf isotopic model can be easily implemented in global models.

In BEPS–EASS, photosynthesis is calculated based on Farquhar's leaf-level model (Farquhar, von Caemmerer & Berry 1980) with an upscaling procedure through sunlit (i = 1) and shaded (i = 2) leaf stratification. The net carboxylation rate of the big leaf is calculated as the minimum of

$$A_{c,i} = V_{c\max}\frac{C_{c,i} - \Gamma_i^*}{C_{c,i} + K_c(1 + O_{c,i}/K_o)}, \quad (1)$$

and

$$A_{j,i} = J\frac{C_{c,i} - \Gamma_i^*}{4\left(C_{c,i} + 2\Gamma_i^*\right)}, \quad (2)$$

where $A_{c,i}$ and $A_{j,i}$ are ribulose 1,5-bisphosphate carboxylase/oxygenase (Rubiso)-limited and ribulose 1,5-Bisphosphate (RuBP)-limited gross photosynthesis rates (μmol m^{-2} s^{-1}), respectively. $V_{c\ max}$ is the maximum carboxylation rate (μmol m^{-2} s^{-1}); J is the electron transport rate (μmol m^{-2} s^{-1}); $C_{c,i}$ and $O_{c,i}$ are the intercellular CO_2 and O_2 mole fractions (mol mol^{-1}), respectively; Γ_i^* is the CO_2 compensation point without dark respiration (mol mol^{-1}); K_c and K_o are Michaelis–Menten constants for CO_2 and O_2 (mol mol^{-1}), respectively.

The net photosynthetic rate is calculated as

$$A_{net,i} = \min(A_{c,i}, A_{j,i}) - R_d, \quad (3)$$

where R_d is the daytime leaf dark respiration and is computed as $R_d = 0.015\ V_{c\ max}$.

The bulk stomatal conductance of the sunlit and shaded leaves for water vapour ($g_{s,i}$, in mol m^{-2} s^{-1}) is calculated using a modified version of the Ball–Woodrow–Berry (Ball, Woodrow & Berry 1987) empirical model following Wang & Leuning (1998):

$$g_{s,i} = g_{o,i} + \frac{mf_w A_{net,i}}{C_{s,i}(1 + D_{s,i}/D_o)}, \quad (4)$$

where $g_{o,i}$ is the residual conductance (mol m^{-2} s^{-1}); $C_{s,i}$ is the CO_2 mole fraction at the leaf surface (μmol mol^{-1}); $D_{s,i}$ is the water vapour saturation deficit at the leaf surface (in kPa); D_o is an empirical parameter determining the sensitivity of stomatal conductance to water vapour saturation deficit (in kPa); m is a parameter related to the intercellular CO_2 mole fraction by $C_{i,i}/C_{s,i} = 1 - 1/m$ at maximal stomatal opening (when both $D_{s,i}$ and $g_{o,i}$ are zero and $f_w = 1$); f_w is a parameter describing the sensitivity of $g_{s,i}$ to soil water availability (Appendix A).

The diffusion of CO_2 from the atmosphere into the leaf is described by

$$A_{net,i} = g_{s,i}(C_{s,i} - C_{i,i})/b_{sc} = g_{c,i}(C_a - C_{i,i}), \quad (5)$$

where the b_{sc} is the ratio of the molecular diffusivity of water to that of CO_2 ($b_{sc} = 1.6$); $g_{c,i}$ represents the conductance to intercellular spaces for CO_2 diffusion from the ambient air (in mol m^{-2} s^{-1}); C_a and $C_{i,i}$ are the CO_2 mole fraction of ambient air in the canopy and the intercellular spaces, respectively (in mol mol^{-1}).

Equations 1–5 and the leaf energy balance equations are solved iteratively for $A_{net,i}$, $g_{c,i}$, $C_{i,i}$, $C_{s,i}$, $D_{s,i}$ and leaf temperatures. The iteration will stop when the difference in temperature between two successive iterations is <0.01 °C for either sunlit or shaded leaves (Wang & Leuning 1998).

In BEPS–EASS, the photosynthetic discrimination against ^{13}C (Δ, in per mille, ‰) for sunlit or shaded leaves is calculated using the widely accepted leaf-level model of ^{13}C discrimination (Farquhar, O'Leary & Berry 1982; Farquhar *et al.* 1989), which is a simple but effective means for ^{13}C discrimination estimation. It neglects the effects of photorespiration and daytime leaf respiration on net discrimination, and implicitly accounts for CO_2 transfer inside the leaf and fixation by using a lower value of the biochemical fractionation parameter b than would be the case for Rubisco (Farquhar *et al.* 1982; Farquhar & Richards 1984):

$$\Delta_i = b - \frac{(b-a)A_{net,i}}{g_{c,i}C_a} = a + (b-a)\frac{C_{i,i}}{C_a}, \quad (6)$$

where b is the weighted ^{13}C fractionation during internal transfer of CO_2 and fixation by Ru*P*2 and phoenopyruvate (PEP) carboxylases applied to C_i, ranging from 26.4 to 28.2‰ for C_3 plants (Lloyd *et al.* 1996) (b is set to be 27.4‰ in this study), and a is the ^{13}C fractionation during diffusion through the stomata (=4.4‰; Craig 1953). The CO_2 mole fraction of ambient air in the canopy (C_a) is simulated using VDS at each time step of 30 s (Chen *et al.* 2004; Chen, Chen & Worthy 2005), instead of simply assuming it be a constant in previous models (e.g. Suits *et al.* 2005). These 30 s high frequency C_a data are averaged to hourly and transferred to BEPS–EASS model.

The integrated canopy-level discrimination (Δ_{canopy}) is assumed to be the flux-weighted average of net carbon assimilation:

$$\Delta_{canopy} = \frac{\sum_{i=1}^{2} \Delta_i A_{net,i} L_i}{\sum_{i=1}^{2} A_{net,i} L_i}, \quad (7)$$

where L_i is the leaf area index for sunlit ($i = 1$) and shaded ($i = 2$) leaves. Partition of the total L into sunlit and shaded portions is a function of cosine of solar zenith angle (β_z) and clumping index (Ω) (Norman 1982; Chen *et al.* 1999),

$$L_1 = 2\cos\beta_z[1 - \exp(-0.5\Omega L/\cos\beta_z)], \quad (8)$$

$$L_2 = L - L_1. \quad (9)$$

Conservation of mass has been used to describe the net exchange of CO_2 and $^{13}CO_2$ between ecosystems and the atmosphere (Flanagan *et al.* 1996; Lloyd, *et al.* 1996, 2001; Yakir & Wang 1996; Bowling, Tans & Monson 2001; Bowling, Pataki & Ehleringer 2003a; Lai *et al.* 2003; Ogée *et al.* 2003). The net ecosystem production (*NEP*) results as the difference between F_A (gross primary productivity minus daytime foliar respiration) and respiration F_R (non-foliar respiration if in daytime), that is, $NEP = F_A - F_R$, both F_A and F_R are positive. If F_A and F_R carry different CO_2 isotope signatures (it is often the case in nature), the total CO_2 mass balance and the isotopic (i.e. $^{13}CO_2$) mass balance equations are not proportional. Following the notation used by Bowling *et al.* (2003a), we can express the isoflux ($F_{\delta 13}$ in μmol m^{-2} s^{-1}‰) as

$$\begin{aligned} F_{\delta 13} &= -(\delta^{13}C_a - \Delta_{canopy})F_A + \delta^{13}C_R F_R \\ &= -(\delta^{13}C_a - \Delta_{canopy})F_A + \delta^{13}C_R^h R_h + \delta^{13}C_R^a R_a, \end{aligned} \quad (10)$$

where $\delta^{13}C_R$, $\delta^{13}C_R^h$ and $\delta^{13}C_R^a$ are stable carbon isotopic signatures of F_R, of heterotrophic respiration flux (R_h) and of autotrophic respiration flux (excluding foliar respiration if in daytime), respectively; $\delta^{13}C_a$ is the carbon isotopic signature of ambient CO_2 in the canopy. Similar to C_a, $\delta^{13}C_a$ is simulated using VDS at each time step (Chen *et al.* 2006b). All terms in δ notation and Δ_{canopy} are in per mille (‰), and CO_2 fluxes are in μmol m^{-2} s^{-1}. The parameterization for stable carbon isotopic signatures of respired CO_2 ($\delta^{13}C_R$, $\delta^{13}C_R^h$ and $\delta^{13}C_R^a$) are discussed in Appendix B.

Data used to drive and test the model

The model is forced by near-surface meteorological variables, including air temperature (T_a), air relative humidity (RH), in-coming shortwave radiation (RAD), wind speed (u) and precipitation (P). A 14 year data series (1990–1996 and 1998–2004) measured on the Fraserdale tower is used to explore inter-annual temporal variations of ecosystem-level carbon discrimination in response to environmental factors. Most of the meteorological forcing data are available for this site. T_a is measured at four levels (1.5, 10.0, 20.0 and 40.0 m), while RH and u are measured at three levels (1.5, 20.0 and 40.0 m; and 10, 20 and 40 m, respectively). Gaps with no valid data at any level are less than 10% year round. In this study, small data gaps of 1–2 h are filled by linear interpolation. When gaps ≥3 h and there is at least one level of data available, gaps are filled by vertical interpolation. Unfortunately, for the Fraserdale tower, precipitation was not measured and incoming shortwave radiation was not available for the period 1990–1996. We used the precipitation data measured at the weather station of Kapuskasing (87 km southwest of Fraserdale) as a proxy. In order to estimate solar irradiance, when the data were not available (e.g. 1990–1996), a solar irradiance module was used after modifying the Bristow–Campbell algorithm, through which the total daily solar irradiance (R_s) was calculated from the limited data set of daily maximum and minimum air temperature and daily total precipitation, along with site latitude, elevation and annual mean temperature (Bristow & Campbell 1984; Winslow, Hunt & Piper 2001) (for detail, see Appendix A in Chen, Chen & Worthy 2005).

The land surface data, including vegetation and soil data, are also needed as model inputs. Most vegetation parameters, such as land cover type (LC), leaf area index (L) and foliage clumping index (Ω) are derived from satellite images instead of directly using observed canopy data. LC and L are derived from satellite images at 1 km resolution (directly from Advanced Very High Resolution Radiometer (AVHRR) images, or upscaling from Landsat TM) (Cihlar *et al.* 1999; Chen *et al.* 2002). Ω is derived from multi-angular POLDER 1 data (Chen, Menges & Leblanc 2005). Ω is an important parameter for partitioning L into sunlit and shaded groups. Biases in Ω estimation, therefore, will affect the simulation of water, heat, carbon as well as photosynthetic discrimination. Data on soil texture (silt and clay fraction) and carbon pools were obtained from the Soil Landscapes of Canada (SLC) database, versions 1.0 and 2.0 (Shields *et al.* 1991; Schut *et al.* 1994; Lacelle 1997).

The Globalview reference marine boundary layer (MBL) data for CO_2 and $\delta^{13}C$ (GLOBALVIEW-CO_2, 2005; Masarie & Tans 1995) were used as the top boundary conditions (i.e. the values in the free troposphere). We used a linear interpolation method to extract these values at the same latitude and times as the study site.

Eight intensive campaigns for flask air sampling were conducted in different seasons during the period of 1998 through 2000 at this site (Huang *et al.* 2003). Each campaign lasted for 3–6 d, with a sampling frequency of 2 h. Air samples were taken in 2 L flasks at the 20 m level of the tower. The flasks were pressurized up to 103.5 kPa above ambient pressure and were dried cryogenically (–70 °C) to remove water vapour. Almost all the samples from the campaigns were analysed within 2 months. CO_2 from each 2 L sample was extracted cryogenically in a vacuum system and was followed by isotopic ratio mass spectrometer (IRMS) analysis (MAT252, Finnigan, Bremen, Germany). The isotopic measurements were directly traced back to the

primary standard VPDB (Huang *et al.* 2003). The assigned ratio for the primary standard (VPDB CO_2) was 0.0112372 for carbon (Allison, Francey & Meijer 1995). The accuracy and precision (including vacuum extraction and IRMS measurements) were 0.02 ‰ for $\delta^{13}C$ (Huang *et al.* 2003).

All the night-time data in the campaigns (1998–2000) at the Fraserdale site were used for deriving the isotopic signature of ecosystem respiration (Appendix B). The measured CO_2 mixing ratio on tower and all the $\delta^{13}C$ data from campaigns are used for model validation (Chen *et al.* 2006a).

RESULTS

Temporal variations

Diurnal trends

Modelled diurnal variations in carbon isotopic discrimination and associated variables for a campaign period (21–23 July 1999) at Fraserdale are shown in Fig. 1 as an example. The greatest discrimination values occurred near sunrise and sunset, while the minima appeared during mid-afternoon (Fig. 1a). A_{net} and g_c had opposite diurnal patterns from Δ, with the maxima occurring around midday and the minima during the early morning and late afternoon (Fig. 1b,c). Patterns of isofluxes were similar to $A_{net,i}$ and $g_{c,i}$ with a midday peak of 400 μmol $m^{-2}s^{-1}$‰ (Fig. 1d). The model has the capacity of capturing the overall diurnal variations of $\delta^{13}C$ in the surface layer [$r^2 = 0.76$, the root mean square error (RMSE) = 0.34‰, sample number (n) = 40]. The strong opposing influences of respiration and photosynthesis on forest air were apparent. CO_2 was consistently depleted of the heavier ^{13}C isotopologue (more negative $\delta^{13}C$) in the early morning and enriched in the late afternoon (Fig. 1e).

In Fig. 2 and Table 1, we examine the overall diurnal patterns of Δ and vapour pressure deficit (VPD) over the 14 year period (1990–1996 and 1998–2004). The 14–year averaged yearly composite diurnal pattern of photosynthetic discrimination against ^{13}C showed an apparent diurnal

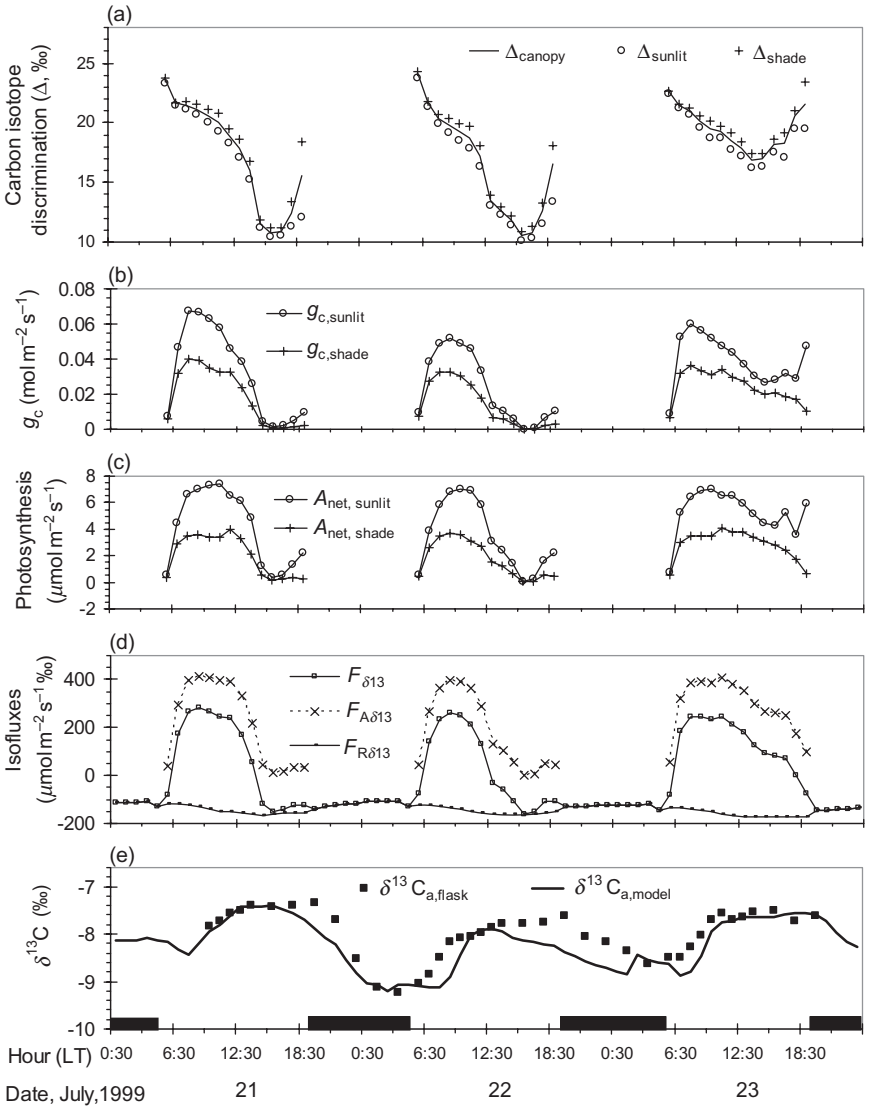

Figure 1. Modelled diurnal variations in carbon isotope discrimination and associated variables for a 3 d campaign (21–23 July 1999) as an example, at Fraserdale tower site. (a) Modelled carbon isotope discrimination of whole canopy (Δ_{canopy}), sunlit leaves (Δ_{sunlit}) and shaded leaves (Δ_{shade}); (b) modelled conductance of CO_2 diffusion from the ambient air to intercellular for the sunlit leaves ($g_{c,sunlit}$) and shaded leaves ($g_{c,shade}$); (c) modelled photosynthetic CO_2 assimilation rate for sunlit leaves ($A_{net,sunlit}$) and shaded leaves ($A_{net,shade}$); (d) modelled isofluxes of $\delta^{13}C$ at the canopy height, which are net isotope flux ($F_{\delta 13}$), isotope flux due to net assimilation ($F_{A\delta 13}$), and isotope flux due to non-foliar respiration ($F_{R\delta 13}$); and (e) modelled ($\delta^{13}C_a$, model) and flask measured ($\delta^{13}C_a$, flask) $\delta^{13}C$ of CO_2 at 20 m height. Dark bars on the horizontal axis denote nocturnal periods.

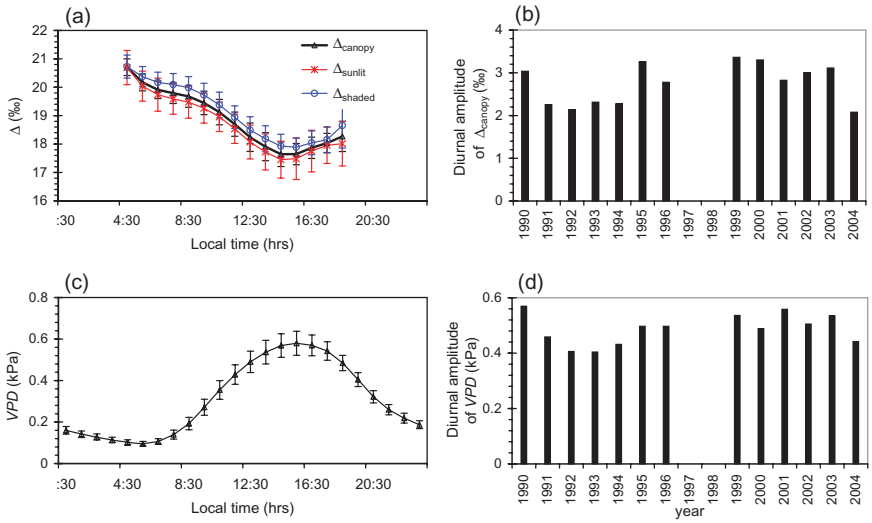

Figure 2. (a) Modelled 14 year averaged yearly composite diurnal patterns of carbon isotope discrimination, (b) modelled mean annual diurnal-amplitude of Δ_{canopy}, (c) measured 14 year averaged yearly composite diurnal patterns of vapour pressure deficit (*VPD*) and (d) measured mean annual diurnal-amplitude of *VPD*. The bars in panels (a) and (c) indicate ±1 SD.

oscillation. Shaded leaves always had larger discrimination values than sunlit leaves. The greatest discrimination occurred near sunrise and sunset, while the minima of Δ typically occurred during the mid-afternoon (1430 ~ 1530 h). After the minima, Δ began to increase until around sunset, at which the SD became the largest (Fig. 2a).

The *VPD* had an approximately opposite diurnal pattern from Δ. The minima were observed around sunrise and sunset, whereas the maxima of 0.58 ± 0.058 kPa were measured during the mid-afternoon (1430 ~ 1630 h) when air temperature was warmest and dry air was entraining from above the PBL. The diurnal maxima and minima of *VPD* during daytime coincided with the minima and maxima of Δ, respectively (Fig. 2a,c). There was a statistically significant correlation ($r^2 = 0.60$, $n = 13$, $P < 0.002$) between mean annual diurnal amplitudes of *VPD* and Δ_{canopy} over the 14 year period (Fig. 2b,d).

As shown in Fig. 3, 14 year overall monthly composite diurnal cycles of Δ_{canopy} and associated variables showed seasonal trends. The largest diurnal amplitude of Δ_{canopy} (3.5–4.8‰) was modelled in the middle growing season (July–August), while the smallest diurnal oscillation (2.5–1.5‰) occurred in the late growing season (September–October) (Fig. 3a). This kind of diurnal pattern of Δ_{canopy} was also found in *VPD*, T_a and *RH* (Fig. 3b–d) and in *NEP*, net isoflux, CO_2 mixing ratio and $\delta^{13}C$ (Fig. 4).

Seasonal trends

In Fig. 5, we examine the 14 year overall seasonal patterns of Δ_{canopy}. The overall seasonality of Δ_{canopy} showed a gradual increasing trend from leaf emergence in May to September and with a slight decrease at the end of the growing season in October (Table 2). There was a noticeable year-to-year variation in seasonality of Δ_{canopy}.

The 14 year overall seasonality of several related meteorological variables measured at 20 m on the tower are shown in Fig. 6 and Table 2. Daytime *VPD* and T_a had similar seasonal patterns with maxima occurring in the middle growing season. However, the inter-annual variation in daytime *VPD* was largest in the early growing season (Table 2). Daytime T_a had a small inter-annual variation during the growing season (±1 SD < 2.5 °C) (Fig. 6b). An apparent seasonal variation of daytime *RH* was also observed with the minima occurring in the early growing season (April–June) and hereafter with a gradual increasing trend to winter (Fig. 6c).

Inter-annual variations

Mean annual air temperature varied from –0.07 °C (1992) to 3.44 °C (2001), and the total annual precipitation during 1990–2004 varied from 710 mm (1998) to 930 mm (1990).

Table 1. Simulated 14 year averaged yearly composite diurnal characteristics of carbon isotope discrimination (mean ± SD, ‰), in the boreal forest in the vicinity of Fraserdale tower, 1990–1996 and 1998–2004[a]

	First maxima occurred around sunrise	Minima occurred during mid-afternoon	Second peaks occurred around sunset	Amplitude
Δ_{sunlit}	20.0 ± 0.5	17.5 ± 0.7	18.0 ± 0.8	2.8 ± 0.6
Δ_{shade}	20.4 ± 0.4	17.9 ± 0.3	18.7 ± 0.8	2.7 ± 0.3
Δ_{canopy}	20.2 ± 0.3	17.7 ± 0.4	18.2 ± 0.5	2.8 ± 0.5

[a]SD and hereafter indicates ±1 SD.

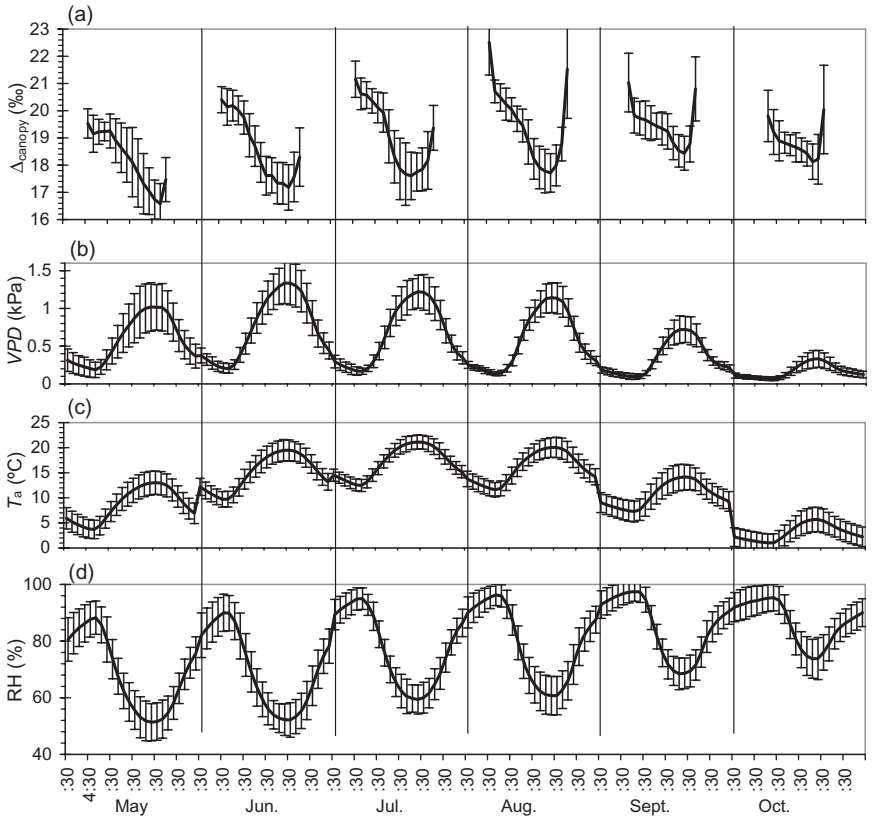

Figure 3. Modelled 14 year averaged monthly composite diurnal cycles of the integrated whole-canopy discrimination Δ_{canopy} and associated variables measured at 20 m height. (a) Modelled Δ_{canopy}, (b) measured vapour pressure deficit (*VPD*), (c) measured temperature (T_a) and (d) measured relative humidity (*RH*). The bars indicate ±1 SD.

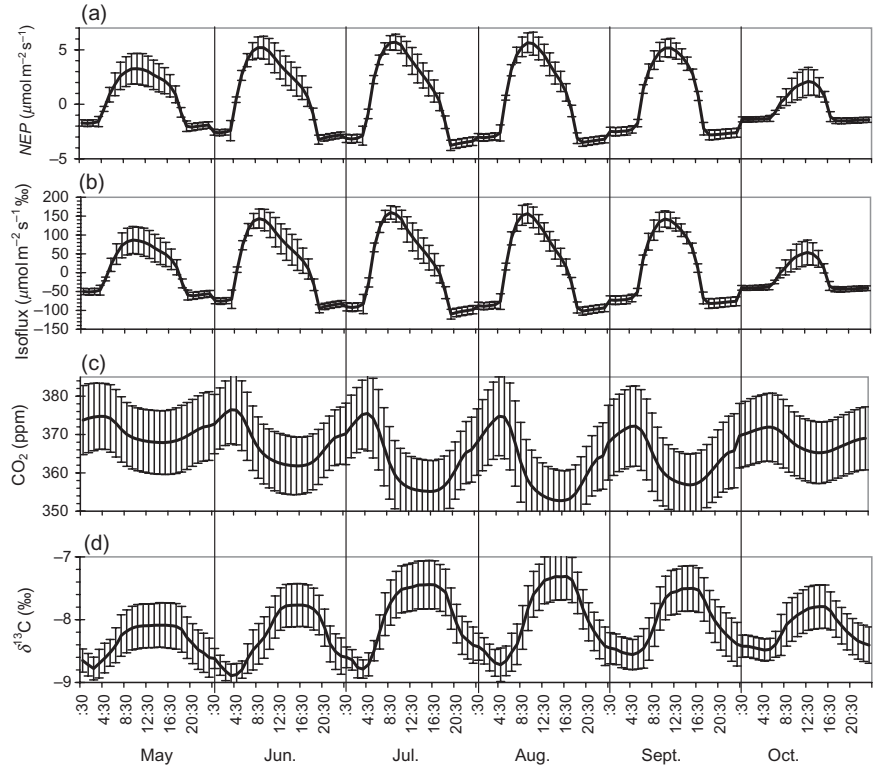

Figure 4. Fourteen year averaged monthly composite diurnal cycles of several variables in the surface layer (a) simulated net ecosystem production (*NEP*) (= $F_A - F_R$), (b) net isoflux, (c) measured CO_2 concentration at 40 m and (d) modelled $\delta^{13}C$ of CO_2 at 20 m. The bars indicate ±1 SD.

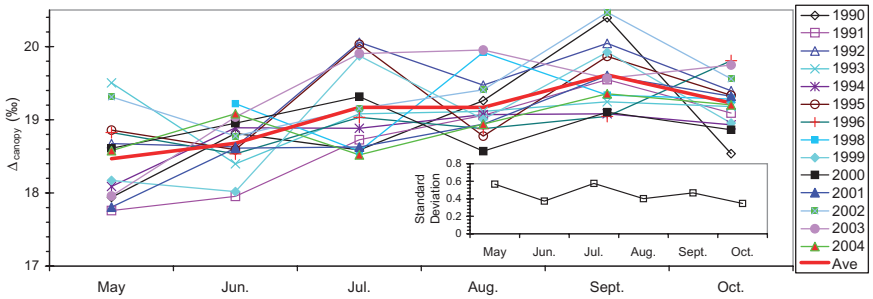

Figure 5. Simulated monthly mean values of photosynthesis discrimination (Δ_{canopy}) for the period of 1990–2004 (1997 excluded), Fraserdale. The thick solid line shows the 14 year average (marked 'ave'). The inset shows the ±1 SD of Δ_{canopy} within these 14 years.

Table 2. Simulated monthly averages (±SD) of canopy-level discrimination Δ_{canopy} and measured daytime vapour pressure deficit (*VPD*), air temperature (T_a) and relative humidity (*RH*) measured during the growing season (May–October) over 14 years (1990–1996 and 1998–2004) in the boreal forest in the vicinity of Fraserdale Tower

	May	June	July	August	September	October	Average
Δ_{canopy} (‰)	18.5 ± 0.6	18.7 ± 0.4	19.2 ± 0.6	19.2 ± 0.4	19.6 ± 0.5	19.2 ± 0.3	19.1 ± 0.5
VPD (kPa)	0.64 ± 0.20	0.84 ± 0.17	0.78 ± 0.15	0.75 ± 0.14	0.46 ± 0.10	0.21 ± 0.06	0.61 ± 0.14
T_a (°C)	9.35 ± 2.27	15.56 ± 1.86	17.77 ± 1.44	17.21 ± 1.53	12.26 ± 2.43	4.41 ± 2.17	12.78 ± 1.95
RH (%)	64.3 ± 5.4	65.3 ± 5.3	71.9 ± 3.3	73.6 ± 4.5	79.8 ± 4.6	82.7 ± 4.8	72.9 ± 4.6

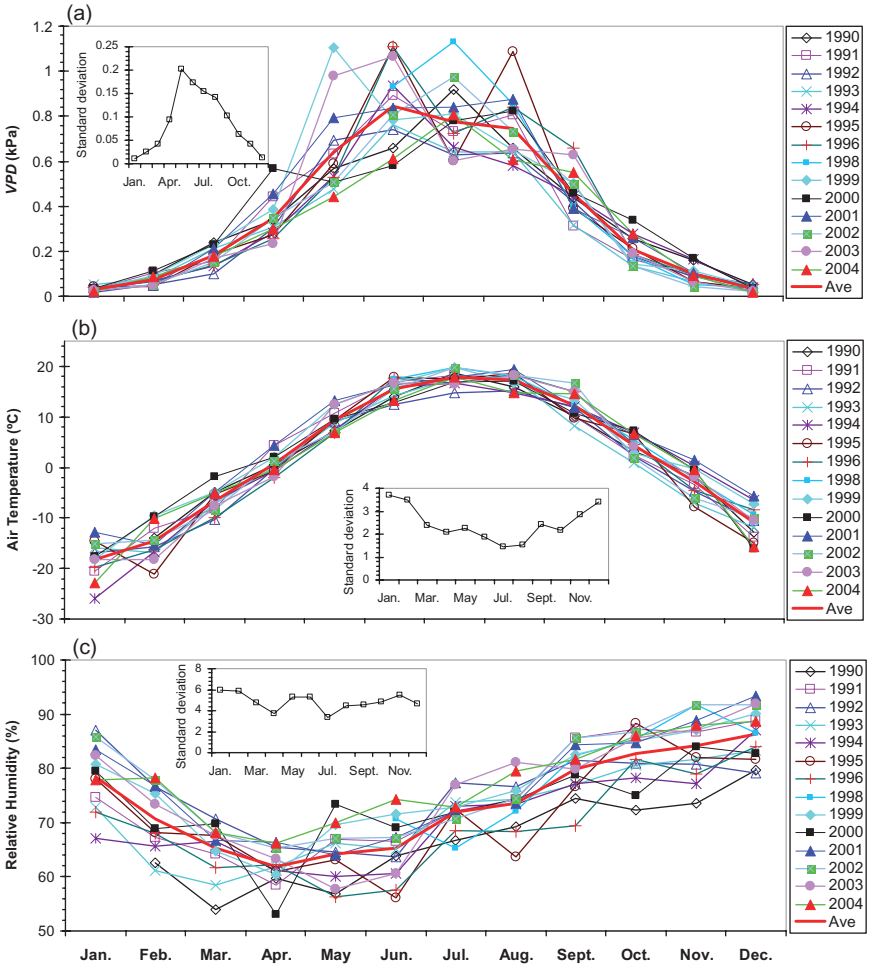

Figure 6. Measured monthly mean values of several meteorological variables at 20 m height, Fraserdale, for the period of 1990–2004 (1997 excluded). (a) Daytime vapour pressure deficit (*VPD*), (b) daytime air temperature (T_a) and (c) daytime relative humidity (*RH*). The thick solid line in each panel shows the 14 year average (marked 'ave').The small figures in each panel show the ±1 SD within these 14 years with regard to the particular variable.

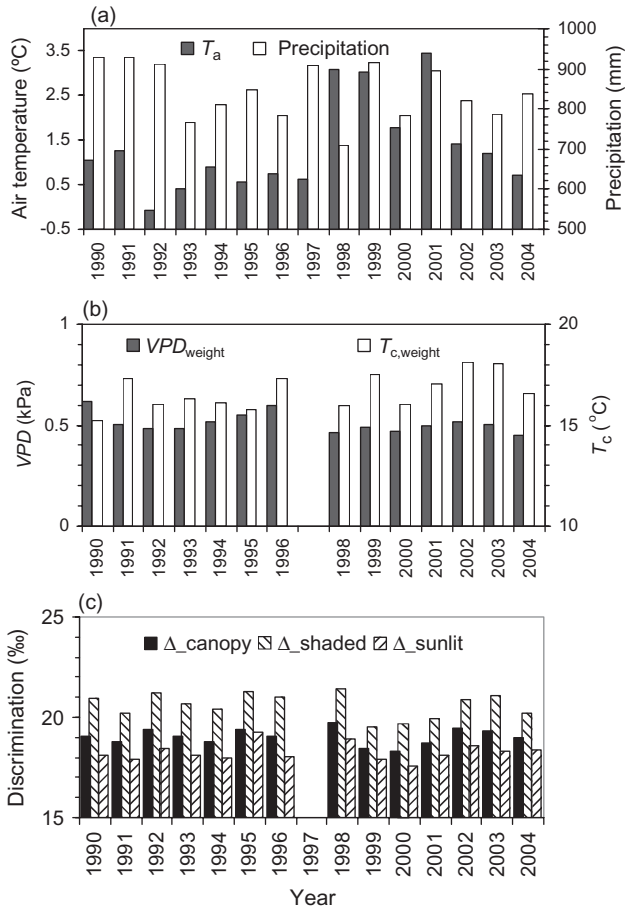

Figure 7. Comparison of simulated annual mean carbon isotope discrimination (c) with several associated variables at Fraserdale site for the period 1990–1996 and 1999–2004. (a) Measured annual mean of 24 h mean air temperature (T_a) and annual total precipitation (the data for 1997–1998 were measured at the weather station Kapuskasing, 87 km southwest of Fraserdale), (b) measured assimilation rate-weighted vapour pressure deficit (VPD_{weight}) and (c) modelled assimilation rate-weighted canopy temperature ($T_{c,weight}$).

The precipitation had a slight decreasing trend, showing a wet period of 1990–1992 (Fig. 7a).

Assimilation rate-weighted meteorological variables (V) are calculated for the analysis of simulated Δ_{canopy} at daily, monthly or yearly time steps using

$$V_{weight} = \sum_{j=1}^{N} VA_{net} \Big/ \sum_{j=1}^{N} A_{net}, \quad \text{if } A_{net} > 0 \tag{11}$$

where V and V_{weight} are hourly value and weighted daily or yearly values, respectively; A_{net} is the whole canopy net photosynthetic rate, which is integrated from sunlit ($i = 1$) and shaded ($i = 2$) leaves, $= \sum_{i=1}^{2} A_{net,i} L_i$; N is the total number of hours for a given averaging time step, for example, for daily, $N = 24$. The measured mean annual assimilation rate-weighted VPD_{weight} varied from 0.45 kPa (2006) to 0.62 kPa (1990) with the 14 year average of 0.51 kPa (Fig. 7b). The modelled 14 year average of assimilation rate-weighted canopy temperature ($T_{c,weight}$) was 16.7 °C with a year-to-year variation within 2.9 °C (Fig. 7b). Mean annual Δ_{canopy} varied from 18.3 to 19.7‰ in the 14 year period. Moreover, Δ_{shaded} was always larger than Δ_{sunlit}, and the differences between them were around 1.5–3‰ (Fig. 7c). The year-to-year variations in the seasonality of Δ_{canopy} and associated variables can be seen from the daily data (Fig. 8). The variations of 24 h mean T_a in summer were much smaller than those in winter over the 14 years (Fig. 8e). The average annual air temperature and mean growing season air temperature had slight increasing trends, showing a warm period of 1998–2001. The observed assimilation rate-weighted VPD_{weight} (Fig. 8b) and relative humidity RH_{weight} (Fig. 8c) had roughly opposite variation trends. During 1991–1996, VPD_{weight} increased while RH_{weight} decreased. The simulated assimilation rate-weighted $T_{c,weight}$ (Fig. 8d) and Δ_{canopy} (Fig. 8a) had no apparent trends but considerable year-to-year changes. Δ_{canopy} tended to have low values in warm years when the assimilation rate-weighted VPD_{weight} values were high (e.g. 1999–2001).

Response to environmental factors

As shown in Fig. 9, a strong negative correlation is modelled between Δ_{canopy} and daytime VPD. On an hourly scale, a second order polynomial described the data with a high correlation coefficient ($r^2 = 0.95$, Fig. 9a), while a linear relationship existed on the daily timescale over the 14 year period ($r^2 = 0.45$, $n = 2066$; Fig. 9b). A linear relationship between daily Δ_{canopy} and assimilation rate-weighted daily VPD_{weight} also existed but was much weaker ($r^2 = 0.15$). As shown in Fig. 10a, the modelled hourly data in 2003 showed that when the mean daytime air temperature T_a was below the threshold of 5–7.5 °C, the instantaneous Δ_{canopy} increased slowly with T_a to its optimum value and then decreased after T_a exceeded the threshold of 5–7.5 °C. This may imply that the physiologically optimum temperature for carbon isotopic discrimination in the boreal ecosystem is 5–7.5 °C. We also find that a second order polynomial can describe the hourly data with $r^2 = 0.48$, $P < 0.001$. A negative linear response of integrated daily Δ_{canopy} to the mean daytime T_a is found from the simulation over the 14 year period ($r^2 = 0.22$, $P < 0.001$; Fig. 10b). Hourly data in 2003 revealed that Δ_{canopy} and the natural logarithm of daytime RH were highly corrected ($r^2 = 0.67$, $n = 1551$). Daily data over the 14 year period showed that Δ_{canopy} was linearly correlated with daytime RH ($r^2 = 0.49$, $n = 2066$). However, it was less well correlated with assimilation rate-weighted daily T_a and RH than with the corresponding unweighted values (r^2: 0.12 versus 0.22 and 0.14 versus 0.49, respectively).

Monthly average Δ_{canopy} had linear correlations with environmental factors. Monthly mean Δ_{canopy} had a significant and positive response to both assimilation rate-weighted and unweighted RH, and their linear correlation coefficients equal 0.59 and 0.60, respectively. Monthly mean Δ_{canopy} had significant negative responses to daytime T_a and daytime

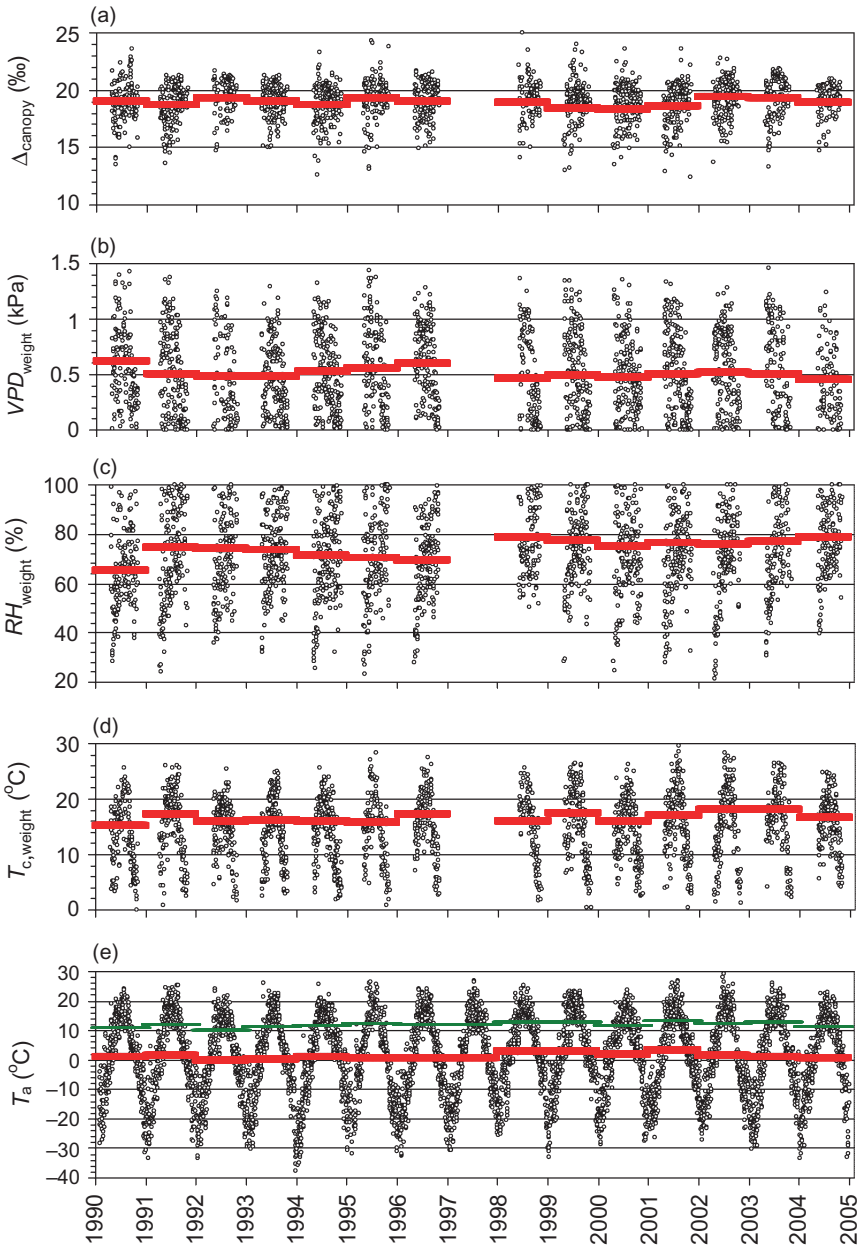

Figure 8. Comparison of simulated daily mean photosynthetic discrimination [Δ_{canopy}, (a)] at Fraserdale site for the periods 1990–1996 and 1999–2004 with several associated variables: daily mean assimilation rate-weighted VPD_{weight} [measured, (b)], relative humidity RH_{weight} [measured, (c)] and canopy temperature $T_{c,weight}$ [modelled, (d)] and measured 24 h mean air temperature [T_a, (e)]. The symbols show the daily mean values and the thick solid lines show the annual mean values for all panels, while the thin solid lines in (e) show the air mean temperature for the growing season. T_a for 1997–1998 was measured at the weather station Kapuskasing, 87 km southwest of Fraserdale.

VPD with linear correlation coefficients of –0.63 and –0.75, respectively (Fig. 11a,b), while it was insignificantly correlated with assimilation rate-weighted T_a and weakly with assimilation rate-weighted VPD_{weight} ($r = -0.52$, $P < 0.05$). The year-to-year variation in Δ_{canopy}, however, only significantly correlated with mean annual air temperature T_a (Fig. 12), while its responses to both assimilation rate-weighted and unweighted *VPD* and *RH* were insignificant.

DISCUSSION

The well-known photosynthesis model of Farquhar *et al.* (1980) has been included in many models to simulate carbon exchange (Bonan 1996; Sellers *et al.* 1996; Baldocchi 1997; Liu *et al.* 1999). A theoretical treatment of carbon isotope discrimination in C_3 photosynthesis (Farquhar *et al.* 1982, 1989; Farquhar & Richards 1984) has also been incorporated into some of these models to permit calculations of ^{13}C discrimination (Baldocchi & Bowling 2003; Suits *et al.* 2005; Aranibar *et al.* 2006; Chen *et al.* 2006a). Canopy-scale models have also been adapted for simulations of within-canopy gradients in the isotopic signature of CO_2, to evaluate $\delta^{13}C$ sampling strategies and the partitioning of net ecosystem carbon exchange into photosynthesis and respiration (Ogée *et al.* 2003, 2004; Baldocchi & Bowling 2005). However, these models are significantly complex.

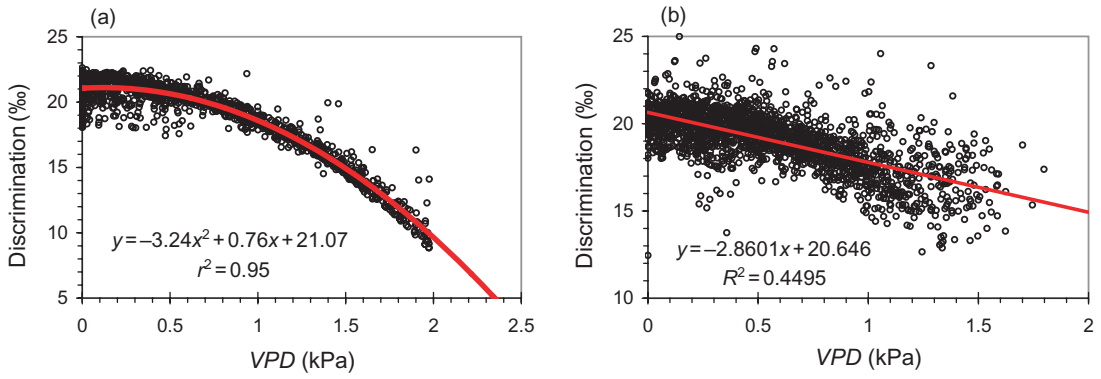

Figure 9. Response of simulated photosynthetic discrimination (Δ_{canopy}) to observed daytime vapour pressure deficit (*VPD*) in a boreal forest in vicinity of Fraserdale site, Ontario, Canada. (a) Hourly data for the year 2003 and (b) daily averaged data for the 14 year period (1990–1996 and 1998–2004).

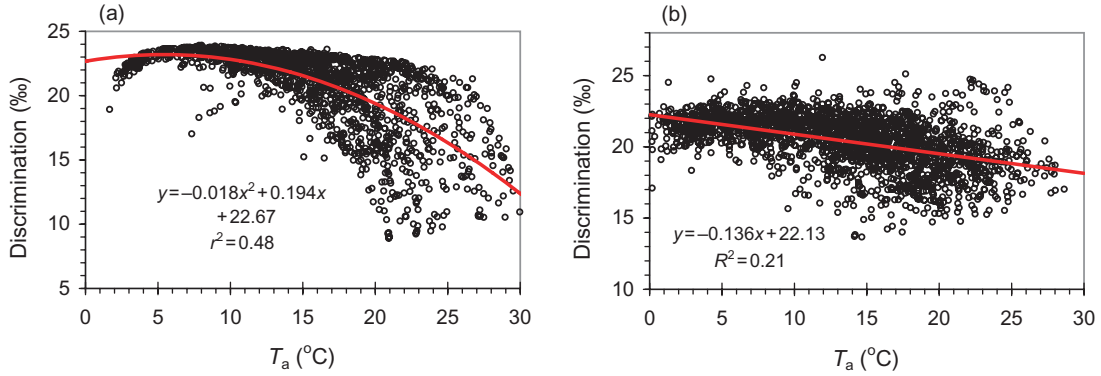

Figure 10. Response of modelled photosynthesis discrimination (Δ_{canopy}) to measured daytime air temperature (T_a) in a boreal forest in vicinity of Fraserdale site, Ontario, Canada. (a) Hourly data for the year 2003 and (b) daily averaged data for the 14 year period (1990–1996 and 1998–2004).

The VDS–BEPS–EASS isotope model used in this study is a one-dimensional integrated ecosystem–boundary layer model, which scales individual leaf-level photosynthetic discrimination up to the canopy level through the separation of sunlit and shaded leaf groups. It has less complexity than the 'multilayer', and such a two-leaf isotopic model can be easily implemented in global models. This approach contrasts with that of simpler 'big-leaf models' (e.g. Lloyd *et al.*

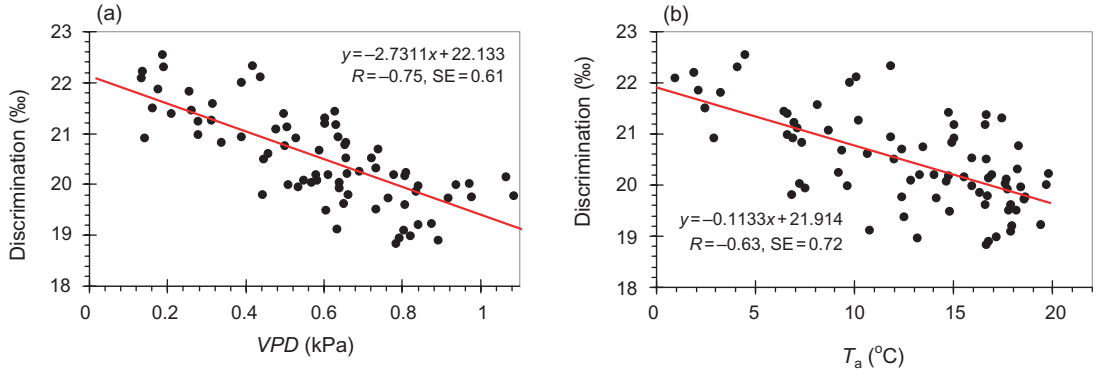

Figure 11. Linear responses of modelled photosynthesis discrimination (Δ_{canopy}) to observed environmental factors on seasonal timescale for the period of 1990–1996 and 1998–2004 in a boreal forest in vicinity of Fraserdale site, Ontario, Canada. (a) Negative correlation between Δ_{canopy} and daytime air temperature (T_a) and (b) negative response of Δ_{canopy} to daytime vapour pressure deficit (*VPD*). SE represents standard error between predicted Δ_{canopy} by the linear regression function and actual Δ_{canopy}.

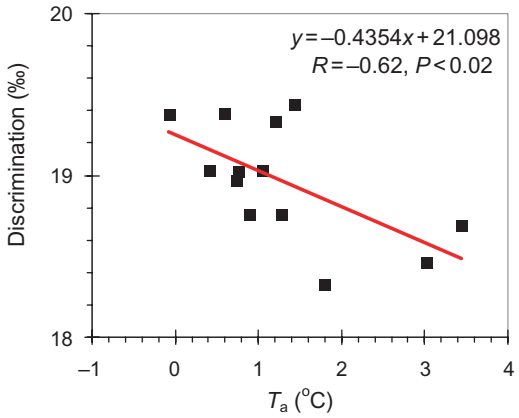

Figure 12. Relationship between simulated annual mean photosynthesis discrimination (Δ_{canopy}) and measured mean annual daytime air temperature (T_a) in a boreal forest in vicinity of Fraserdale site, Ontario, Canada, for the period of 1990–1996 and 1998–2004.

1996), which do not properly consider non-linear biological combinations of the sunlit and shaded leaves. A detailed discussion of this scaling problem was given by De Pury & Farquhar (1997). To simplify model parameterization, we use the simple and widely accepted model (Eqn 6) (Farquhar *et al.* 1982) to calculate Δ. It implicitly accounts for all the fractionation during diffusion and fixation using a lower value for *b* (Farquhar & Richards 1984), instead of explicitly simulating all the fractionation processes occurring during the diffusion of CO_2 from the atmosphere to the sites of carboxylation in leaves, and by fixation of CO_2 in the chloroplasts (Suits *et al.* 2005; Aranibar *et al.* 2006). The CO_2 mole fraction of the ambient air in the canopy (C_a in Eqns 5 & 6) is simulated using VDS at each time step of 30 s (Chen *et al.* 2004, 2005a), instead of assuming it to be a constant in previous models (e.g. Suits *et al.* 2005). The isotopic signature of heterotrophic respiration ($\delta^{13}C_R^h$) is calculated using the Keeling-plot methodology with nighttime data acquired in field campaigns, while that of autotrophic respiration $\delta^{13}C_R^a$ (excluding foliar respiration if in daytime) is computed by model runs (see Appendix B). The differences in $\delta^{13}C$ between plant organs caused by post-photosynthetic fractionation are also considered in the updated model (Appendix B).

This model output has been compared to intensive campaigns (1998–2000) and weekly diurnal sampling data at a boreal forest site (Fraserdale, Canada) with satisfactory results (Chen *et al.* 2006a). Factors contributing to the satisfactory performance of this isotope model include its large model domain through the whole CBL, its dependence on coupled and constraining processes, such as leaf energy exchange, turbulent transfer, photosynthesis and stomatal conductance, and its representation of these processes for separate sunlit and shaded leaf classes.

The overall diurnal cycles of Δ_{canopy} over the 14 year period show that the greatest values of Δ_{canopy} occurred near sunrise (around 20.2 ± 0.3‰), and sunset (about 18.2 ± 0.5‰), while the minima (17.7 ± 0.4‰) were found during mid-afternoon. The 14 year averaged composite diurnal amplitude of Δ_{canopy} was 2.8 ± 0.5‰. This diurnal pattern, high Δ values at down and dusk and low values around midday to mid-afternoon, is similar to that simulated for a temperate broadleaf forest near Oak Ridge, Tennessee (35°57′30″N, 84°17′15 ″W) in 1998 (Baldocchi & Bowling 2003).

This modelled diurnal pattern by the commonly used simple Farquhar *et al.* (1982) model has been observed in two studies: a leaf scale study on *Piper aduncum* in a tropical forest of Trinidad (Harwood *et al.* 1998) and a branch scale observation made for *Picea sitchensis* (Bong.) Carr. in Griffin Forest, an even-aged plantation of Queen Charlotte Islands provenance, near Aberfeldy, Perthshire, UK (56°37″N, 3°48″W) (Wingate *et al.* 2007). Large estimated uncertainties at dawn and dust were reported in Wingate *et al.* (2007), while the largest SDs were only modelled around sunset in this study (Fig. 2a). It is interesting that a consistent diurnal pattern was modelled and observed for different ecosystems and plant types. Wingate *et al.* (2007) highlighted isotopic disequilibria between the gross fluxes of photosynthesis and daytime respiration leading to the pronounced diurnal variability of Δ based on their limited campaign measurements. On the basis of a 14 year data record (observed and simulated), it is likely that the diurnal oscillation of several key variables (i.e. *VDP*, T_a, photosynthetic photon flux density (PPFD) and available soil moisture, etc.) regulating stomatal conductance mainly controls the diurnal variability of Δ: largest Δ_{canopy} values occurred near sunrise and sunset, when photosynthesis rates diminished relative to respiration and the stomata closed, and the CO_2 mole fraction inside the sub-stomatal cavity of leaf approximately equaled to or was larger than that in the ambient air in the canopy. Minimum Δ_{canopy} values typically occurred during mid-afternoon (1400–1500 h), when the day's highest *VPD* occurred because the air temperatures were warmest and dry air was being entrained from above the CBL. These factors led to lower stomatal conductance, independent of the change in photosynthesis, and thereby forced Δ_{canopy} values to be lower. The 14 year averaged composite diurnal amplitude of Δ_{canopy} was 2.8‰ with an inter-annual variation ranging from 2.1 to 3.4‰. The diurnal amplitude of Δ_{canopy} presented seasonal trends as well: large diurnal oscillations occurred in the middle growing season, while small diurnal amplitudes occurred in the late growing season. This kind of seasonality in diurnal cycles of Δ_{canopy} was consistent with *VPD*, T_a, *RH*, *NEP* (Fig. 3) and net isoflux (Fig. 4).

The modelled 14 year overall seasonal trend of Δ_{canopy} in a boreal forest in the vicinity of the Fraserdale tower is consistent with the measurements made in a Douglas-fir forest located on Vancouver Island, British Columbia (49.90°N. 125.37°W; Ponton *et al.* (2006). The observed **Δ** and the carbon isotopic signature of ecosystem-respired CO_2 in the Douglas-fir forest had an increasing trend from the early to middle growing season and a strong decrease at the end of the growing season in 2003 (see Fig. 5 of Ponton *et al.* 2006).

The average annual Δ_{canopy} varied from 18.5 to 19.6‰ with a 14 year average of 19.1 ± 0.5‰, which is consistent with both measured and simulated results for similar ecosystems (e.g. Lai *et al.* 2005; Suits *et al.* 2005; Ponton *et al.* 2006). The modelled diurnal patterns of Δ_{canopy} are also consistent with other estimates in the literatures (e.g. Baldocchi & Bowling 2003).

Non-linear effects of environmental factors, such as light, humidity, temperature and soil moisture, on physiological processes, that is, photosynthesis, transpiration, stomatal conductance and isotopic discrimination, have been recognized. Limited attempts to examine the response of Δ_{canopy} to environmental factors across different temporal scales have yet to be made. In this study, we found that Δ_{canopy} negatively responded to daytime *VPD* and daytime T_a, and positively responded to daytime *RH* from hourly to seasonal timescales. The sensitivities of discrimination to assimilation rate-weighted *VPD*, T_a and *RH* were less than those to unweighted values at daily and seasonal timescales. This could reflect the complex interactions among the effects of meteorological variables on stomatal conductance and the non-linear relationship between stomatal conductance and discrimination. The year-to-year variation in Δ_{canopy}, however, only significantly correlated with mean annual daytime T_a. Moreover, we found that there were no significant differences between correlations of Δ_{canopy} and Δ_{leaf} to environmental variables in the boreal forest ecosystem. *VPD* is not an independent driving factor of stomatal conductance in the model. *VPD* is related to T_a and *RH*, and can also be correlated with radiation, and their effects are considered in simulating photosynthesis and stomatal conductance. The same values of *VPD* may result under different combinations of radiation, T_a and *RH*, giving rise to different Δ_{canopy} values for a given *VPD*. This is also noted in the study on the simulation of isotope discrimination in a broadleaf forest with a multilayer canopy model (Baldocchi & Bowling 2003), showing a negative relationship between photosynthetically active radiation and hourly discrimination during the growing season. In their study, the discrimination varied by 4–6‰ for a given value of photon flux density, reflecting the interactions among different factors (i.e. cloudiness and *VPD*) determining stomatal conductance, photosynthesis and discrimination. Thus, different relations between *VPD* or other meteorological variables and observed discrimination can naturally occur at different sites and times, without indicating a difference in the controlling mechanisms of ecosystem discrimination. A strong climatic control on stomatal regulation of ecosystem isotope discrimination is implied by the present data across hourly to inter-annual timescales in this study.

CONCLUSIONS

By applying a combined ecosystem–boundary layer isotope model to a 14 year series of data at a boreal forest site, the variability of canopy-level carbon discrimination and its response to environmental factors on multiple timescales are explored in this study. The following conclusions are drawn:

1 The general diurnal trend of Δ_{canopy} is maxima occurring at dawn and dusk, while minima occurring during mid-afternoon. Both A_{net} and g_c showed opposite diurnal patterns from Δ_{canopy}.
2 The overall seasonality of Δ_{canopy} shows a gradual increasing trend from leaf emergence in May to September and with a slight decrease at the end of the growing season in October.
3 Δ_{canopy} negatively responded to *VPD* and T_a, and positively responded to *RH* from hourly to seasonal timescales. On the decadal scale, mean annual daytime temperature was significantly correlated with Δ_{canopy}, but mean annual daytime *VPD* and *RH* were not.

ACKNOWLEDGMENTS

The authors would like to acknowledge the funding support from the Canadian Foundation for Climate and Atmospheric Sciences (project GC423). We would like to acknowledge Doug Worthy and M. Ernst (Meterological Service of China) for the measurements of the CO_2 concentration and meteorology data at Faserdale. We are grateful to Lin Huang for the isotope campaign data and Pieter Tans and K. Masarie at the National Oceanic & Atmospheric Administration/Climate Monitoring & Diagnostics Laboratory (NOAA/CMDL) Carbon Cycle Group for creating and updating the MBL reference fields of CO_2 and $\delta^{13}C$. We also gratefully acknowledge constructive and insightful suggestions/comments by Dr Farquhar (the subject editor) and three anonymous reviewers, which greatly improved the presentation of our results.

REFERENCES

Allison C.E., Francey R.J. & Meijer H.A.J. (1995) Recommendations for the reporting of stable isotope measurements of carbon and oxygen in CO_2 gas, in Reference and Intercomparison Materials for Stable Isotopes of Light Elements. *International Atomic Energy Agency (IAEA)-Tecdoc* **825,** 155–162.

Aranibar J.N., Berry J.A., Riley W.J., Pataki D.E. & Ehleringer J.R. (2006) Combining meteorology, eddy fluxes, isotope measurements, and modeling to understand environmental controls of carbon isotope discrimination at the canopy scale. *Global Change Biology* **12,** 710–730.

Badeck F.W., Tcherkez G., Nogués S., Clément P.N. & Ghashghaie J. (2005) Post-photosynthetic fractionation of stable carbon isotopes between plant organs—a widespread phenomenon. *Rapid Commununications in Mass Spectrometry* **19,** 1381–1391.

Baldocchi D.D. (1997) Measuring and modeling carbon dioxide and water vapour exchange over a temperate broad-leaved forest during the 1995 summer drought. *Plant, Cell & Environment* **20,** 1108–1122.

Baldocchi D.D. & Bowling D.R. (2003) Modeling the discrimination of ^{13}C above and within a temperate broad-leaved forest canopy on hourly to seasonal time scales. *Plant, Cell & Environment* **26,** 231–244.

Baldocchi D.D. & Bowling D.R. (2005) Theoretical examination of keeling-plot relationships for carbon dioxide in a temperate

broadleaved forest with a biophysical model, CANISOTOPE. In *Stable Isotopes and Biosphere-Atmosphere Interactions: Processes and Biological Controls* (eds L.B. Flanagan, J.R. Ehleringer, D.E. Pataki & H.A. Mooney), pp. 109–124. Elsevier Press, San Diego, CA, USA.

Ball J.T., Woodrow I.E. & Berry J.A. (1987) A model predicting stomatal conductance and its contribution to the control of photosynthesis under different environmental conditions. In *Progress in Photosynthesis Research* (ed. J. Biggins), pp. 221–224. Martinus Nijhoff Publishers, Dordrecht, the Netherlands.

Battle M., Bender M.L., Tans P.P., White J.W.C., Ellis J.E., Conway T. & Francey R.J. (2000) Global carbon sinks and their variability inferred from atmospheric O_2 and $\delta^{13}C$. *Science* **287,** 2467–2470.

Bonan G.B. (1991) A biophysical surface-energy budget analysis of soil-temperature in the boreal forests of interior Alaska. *Water Resources Research* **27,** 767–781.

Bonan G.B. (1996) *A Land Surface Model (LSM version 1.0) for Ecological, Hydrological, and Atmospheric Studies: Technical Description and User's Guide*. National Center for Atmospheric Research, Boulder, CO, USA.

Bowling D.R., Tans P.P. & Monson R.K. (2001) Partitioning net ecosystem carbon exchange with isotopic fluxes of CO_2. *Global Change Biology* **7,** 127–145.

Bowling D.R., McDowell N.G., Bond B.J., Law B.E. & Ehleringer J.R. (2002) ^{13}C content of ecosystem respiration is linked to precipitation and vapor pressure deficit. *Oecologia* **131,** 113–124.

Bowling D.R., Pataki D.E. & Ehleringer J.R. (2003a) Critical evaluation of micrometeorological methods for measuring ecosystem-atmosphere isotopic exchange of CO_2. *Agricultural and Forest Meteorology* **116,** 159–179.

Bowling D.R., Sargent S.D., Tanner B.D. & Ehleringer J.R. (2003b) Tunable diode laser absorption spectroscopy for stable isotope studies of ecosystem-atmosphere CO_2 exchange. *Agricultural and Forest Meteorology* **118,** 1–19.

Bristow K.L. & Campbell G.S. (1984) On the relationship between incoming solar radiation and daily maximum and minimum temperature. *Agricultural and Forest Meteorology* **31,** 159–166.

Canadell J.G., Mooney H.A., Baldocchi D.D., *et al* (2000) Carbon metabolism of the terrestrial biosphere: a multitechnique approach for improved understanding. *Ecosystems* **3,** 115–130.

Chen B., Chen J.M. & Ju W. (2007) Remote sensing based ecosystem-atmosphere simulation scheme (EASS) – model formulation and test with multiple-year data. *Ecological Modelling* (in press).

Chen J.M., Liu J., Cihlar J. & Guolden M.L. (1999) Daily canopy photosynthesis model through temporal and spatial scaling for remote sensing applications. *Ecological Modelling* **124,** 99–119.

Chen J.M., Pavlic G., Brown L., *et al* (2002) Derivation and validation of Canada-wide coarse-resolution leaf area index maps using high resolution satellite imagery and ground measurements. *Remote Sensing of Environment* **80,** 165–184.

Chen B., Chen J.M., Liu J., Chan D., Higuchi K. & Shashkov A. (2004) A vertical diffusion scheme to estimate the atmospheric rectifier effect. *Journal of Geophysical Research-Atmospheres* **109,** D04306. doi:10.1029/2003JD003925

Chen B., Chen J.M. & Worthy D. (2005) Interannual variability in the atmospheric CO_2 rectification over a boreal forest region. *Journal of Geophysical Research-Atmospheres* **110,** D16301. doi:10.1029/2004JD005546

Chen J.M., Menges C.H. & Leblanc S.G. (2005) Global mapping of foliage clumping index using multi-angular satellite data. *Remote Sensing of Environment* **97,** 447–457.

Chen B., Chen J.M., Tans P.P. & Huang L. (2006a) Modeling dynamics of stable carbon isotopic exchange between a boreal ecosystem and the atmosphere. *Global Change Biology* **12,** 1842–1867. doi:10.1111/j.1365-2486.2006.01200.x

Chen B., Chen J.M., Huang L. & Tans P.P. (2006b) Simulating dynamics of $\delta^{13}C$ of CO_2 in the planetary boundary layer over a boreal forest region: covariation between surface fluxes and atmospheric mixing. *Tellus B* **58,** 537–549.

Chen B., Chen J.M., Gang M., Yuen C-W., Higuchi K. & Chan D. (2007) Modeling and scaling coupled energy, water, and carbon fluxes based on remote sensing: an application to Canada's landmass. *Journal of Hydrometeorology* **8,** 123–143.

Ciais P., Tans P.P., Trolier M., White J.W.C. & Francey R.J. (1995a) A large Northern Hemisphere terrestrial CO_2 sink indicated by the $^{13}C/^{12}C$ ratio of atmospheric CO_2. *Science* **269,** 1098–1102.

Ciais P., Tans P.P., White J.W.C., Trolier M., Francey R.J., Berry J.A., Randall D., Sellers P., Collatz J. & Schimel D. (1995b) Partitioning of ocean and land uptake of CO_2 as inferred by $\delta^{13}C$ measurements from NOAA Climate Monitoring and Diagnostics Laboratory Global Air Sampling Network. *Journal of Geophysical Research-Atmospheres* **100,** 5051–5070.

Cihlar J., Beaubien J., Latifovic R. & Simard G. (1999) Land cover of Canada 1995 version 1.1. Digital data set documentation. Natural Resources Canada, Ottawa, Ontario, Canada. ftp://ftp2.ccrs.nrcan.gc.ca/ftp/ad/EMS/landcover95/ [Date of access: 9 July 2007].

Craig H. (1953) Carbon-13 in plants and the relationships between carbon-13 and carbon-14 variations in nature. *The Journal of Geology* **62,** 115–149.

De Pury D.G.G. & Farquhar G.D. (1997) Simple scaling of photosynthesis from leaves to canopies without the errors of big-leaf models. *Plant, Cell & Environment* **20,** 537–557.

Farquhar G.D. & Richards R.A. (1984) Isotopic composition of plant carbon correlates with water use efficiency of wheat genotypes. *Australian Journal of Plant Physiology* **11,** 539–552.

Farquhar G.D., von Caemmerer S. & Berry J.A. (1980) A biochemical model of photosynthetic CO_2 assimilation in leaves of C_3 species. *Planta* **149,** 78–90.

Farquhar G.D., O'Leary M.H. & Berry J.A. (1982) On the relationship between carbon isotope discrimination and the intercellular carbon dioxide concentration in leaves. *Australian Journal of Plant Physiology* **9,** 121–137.

Farquhar G.D., Ehleringer J.R. & Hubick K.T. (1989) Carbon isotope discrimination and photosynthesis. *Annual Review of Plant Physiology and Plant Molecular Biology* **40,** 503–537.

Flanagan L.B., Brooks J.R., Varney G.T., Berry S.C. & Ehleringer J.R. (1996) Carbon isotope discrimination during photosynthesis and the isotope ratio of respired CO_2 in boreal forest ecosystems. *Global Biogeochemical Cycles* **10,** 629–640.

Fung I., Field C.B., Berry J.A., *et al* (1997) Carbon 13 exchanges between the atmosphere and the biosphere. *Global Biogeochemical Cycles* **11,** 507–533.

GLOBALVIEW-CO_2. (2005) Cooperative Atmospheric Data Integration Project: carbon dioxide. [CD-ROM]. NOAA Climate Monitoring and Diagnostics Laboratory, Boulder, CO, USA (Available via anonymous FTP to ftp.cmdl.noaa.gov, Path: ccg/co2/GLOBALVIEW) [Date of access: 9 July 2007].

Griffis T.J., Baker J.M., Sargent S.D., Tanner B.D. & Zhang J. (2004) Measuring field-scale isotopic CO_2 fluxes with tunable diode laser absorption spectroscopy and micrometeorological techniques. *Agricultural and Forest Meteorology* **124,** 15–29.

Griffis T.J., Baker J.M. & Zhang J. (2005) Seasonal dynamics and partitioning of isotopic CO_2 exchange in a C_3/C_4 managed ecosystem. *Agricultural and Forest Meteorology* **132,** 1–19.

Harwood K.G., Gillon J.S., Griffiths H. & Broadmeadow M.S.J. (1998) Diurnal variation of $\Delta^{13}CO_2$, $\Delta C^{18}O^{16}O$ and evaporative site enrichment of $\delta H_2{}^{18}O$ in *Piper aduncum* under field conditions in Trinidad. *Plant, Cell & Environment* **21,** 269–283.

Higuchi K., Worthy D. & Chan D., *et al* (2003) Regional source/sink impact on the diurnal, seasonal and inter-annual variations in atmospheric CO_2 at a boreal forest site in Canada. *Tellus B* **55,** 115–125.

Huang L., Norman A.L., Allison C.E., Francey R.J., Ernst D., Chivulescu A. & Higuchi K. (2003) Traceability – maintenance for high precision stable isotope measurement ($\delta^{13}C$ & $\delta^{18}O$) of Air-CO2 by Lab-Carbonate-Standards at MSC: application to the Inter-Comparision Program (alert, Canada) with CSIRO. In *The Report to the 11th WMO/IAEA Meeting of Experts on CO_2 Concentration and Related Tracer Measurement Techniques*, No. 148, pp. 9–16, September 2001, Tokyo, Japan.

Joos F. & Bruno M. (1998) Long-term variability of the terrestrial and oceanic carbon sinks and the budgets of the carbon isotopes ^{13}C and ^{14}C. *Global Biogeochemical Cycles* **12,** 277–296.

Kaplan J.O., Prentice I.C. & Buchmann N. (2002) The stable carbon isotope composition of the terrestrial biosphere: modeling at scales from the leaf to the globe. *Global Biogeochemical Cycles* **16,** 1060. doi:10.1029/2001GB001403

Keeling CD, Piper S.C., Bacastor R.B., Wahlen M., Whorf T.P., Heimann M. & Meijer H.A. (2001) *Exchanges of Atmospheric CO_2 and $^{13}CO_2$ with the Terrestrial Biosphere and Oceans from 1978 to 2000: I. Global Aspects, SIO Ref. Ser. 01–06*, pp.1–45. Scripps Institution of Oceanography, San Diego, CA, USA.

Lacelle B. (1997) Canada's soil organic carbon database. In *Soil Processes and the Carbon Cycle* (eds R. Lal, J. Kimbla, R.F. Follett & B.A. Stewart) pp. 93–102. CRC Press, New York, NY, USA.

Lai C.T., Schauer A.J., Owensby C., Ham J.M. & Ehleringer J.R. (2003) Isotopic air sampling in a tallgrass prairie to partition net ecosystem CO_2 exchange. *Journal of Geophysical Research* **108,** 4566. doi:10.1029/2002JD003369

Lai C.T., Ehleringer J.R., Tans P.P., Wofsy S.C., Urbanski S.P. & Hollinger D.Y. (2004) Estimating photosynthetic ^{13}C discrimination in terrestrial CO_2 exchange from canopy to regional scales. *Global Biogeochemical Cycles* **18,** GB1041. doi:10.1029/2003GB002148

Lai C.T., Ehleringer J., Schauer A., Tans P.P., Hollinger D., Paw K.T.U., Munger J. & Wofsy S. (2005) Canopy-scale $\delta^{13}C$ of photosynthetic and respiratory CO_2 fluxes: observations in forest biomes across the United States. *Global Change Biology* **11,** 633–643. doi: 10.1111/j.1365-2486.2005.00931.x

Lai C.T., Riley W., Owensby C., Ham J., Schauer A. & Ehleringer J. (2006) Seasonal and interannual variations of carbon and oxygen isotopes of respired CO_2 in a tallgrass prairie: measurements and modeling results from three years with contrasting water availability. *Journal of Geophysical Research-Atmospheres*, **111,** D08S06, doi:10.1029/2005JD006436

Liu J., Chen J.M., Cihlar J. & Chen W. (1999) Net primary productivity distribution in BOREAS region from a process model using satellite and surface data. *Journal of Geophysical Research-Atmospheres* **104,** 27735–27754.

Lloyd J., Kruijt B., Hollinger D.Y., *et al* (1996) Vegetation effects on the isotopic composition of atmospheric CO_2 at local and regional scales: theoretical aspects and a comparison between rain forest in Amazonia and a boreal forest in Siberia. *Australian Journal of Plant Physiology* **23,** 371–399.

Lloyd J., Francey R.J., Mollicone D., *et al* (2001) Vertical profiles, boundary layer budgets, and regional flux estimates for CO_2 and its $^{13}C/^{12}C$ ratio and for water vapor above a forest/bog mosaic in central Siberia. *Global Biogeochemical Cycles* **15,** 267–284.

Masarie K.A. & Tans P.P. (1995) Extension and integration of atmospheric carbon dioxide data into a globally consistent measurement record. *Journal of Geophysical Research-Atmospheres* **100,** 11593–11610.

McGuire A.D., Sitch, S., Clein J.S., *et al* (2001) Carbon balance of the terrestrial biosphere in the twentieth century: analyses of CO_2, climate and land-use effects with four process-based ecosystem models. *Global Biogeochemical Cycles* **15,** 183–206.

McManus J.B., Nelson D.D., Shorter J.H., Jimenez R., Herndon S., Saleska S. & Zahniser M. (2005) A high precision pulsed quantum cascade laser spectrometer for measurements of stable isotopes of carbon dioxide. *Journal of Modern Optics* **52,** 2309–2321.

Norman J.M. (1982) Simulation of microclimates. In *Biometeorology in Integrated Pest Management* (eds J.L. Hatfield & I.J. Thomason) pp. 65–99. Academic Press, New York, NY, USA.

Ogée J., Brunet Y., Loustau D., Berbigier P. & Delzon S. (2003) MuSICA, a CO_2, water and energy multi-layer, multi-leaf pine forest model: evaluation from hourly to yearly time scales and sensitivity analysis. *Global Change Biology* **9,** 697–717.

Ogée J., Peylin P., Cuntz M., Bariac T., Brunet Y., Berbigier P., Richard P. & Ciais P. (2004) Partitioning net ecosystem carbon exchange into net assimilation and respiration with canopy-scale isotopic measurements: an error propagation analysis with $^{13}CO_2$ and $CO^{18}O$ data. *Global Biogeochemical Cycles* **18,** GB2019. doi:10.1029/2003GB002166

Ponton S., Flanagan L.B., Alstard K., Johnson B.G., Morgenstern K., Kljun N., Black T.A. & Barr A.G. (2006) Comparison of ecosystem water-use efficiency among Douglas-fir forest, aspen forest and grassland using eddy covariance and carbon isotope techniques. *Global Change Biology* **12,** 294–310.

Randerson J.T., Still C.J., Ballé J.J., *et al* (2002a) Carbon isotope discrimination of arctic and boreal biomes inferred from remote atmospheric measurements and a biosphere-atmosphere model. *Global Biogeochemical Cycles* **16,** 1028. doi:10.1029/2001GB001435

Randerson J.T., Collatz G.J., Fessenden J.E., Munoz A.D., Still C.J., Berry J.A., Fung I.Y., Suits N. & Denning A.S. (2002b) A possible global covariance between terrestrial gross primary production and ^{13}C discrimination: Consequences for the atmospheric ^{13}C budget and its response to ENSO. *Global Biogeochemical Cycles* **16,** 1136. doi:10.1029/2001GB001845

Schauer A.J., Lott M.J., Cook C.S. & Ehleringer J.R. (2005) An automated system for stable isotope and concentration analyses of CO_2 from small atmospheric samples. *Rapid Communications in Mass Spectrometry* **19,** 359–362.

Schut P., Shields J., Tarnocai C., Coote D. & Marshall I. (1994) Soil Landscapes of Canada – An Environmental Reporting Tool Canadian Conference on GIS Proceedings, pp. 953–965, 6–10 June 1994, Ottawa, Canada.

Sellers P.J., Randall D.A., Collatz G.J., *et al* (1996) A revised land surface parameterization (SiB2) for atmospheric GCMs. Part I: model formulation. *Journal of Climate* **9,** 676–705.

Shields J.A., Tarnocai C., Valentine K.W.G. & MacDonald K.B. (1991) *Soil Landscapes of Canada, Procedures Manual and User's Hand Book*. Agric. Can. Publ. 1868/E, Agriculture Canada, Ottawa, Canada.

Suits N.S., Denning A.S., Berry J.A., Still C.J., Kaduk J., Miller J.B. & Baker I.T. (2005) Simulation of carbon isotope discrimination of the terrestrial biosphere. *Global Biogeochemical Cycles* **19,** GB1017. doi:10.1029/2003GB002141

Tans P.P. (1980) On calculating the transfer of carbon-13 in reservoir models of the carbon cycle. *Tellus B* **32,** 464–469.

Tans P.P., Berry J.A. & Keeling R.F. (1993) Oceanic $^{13}C/^{12}C$ observations: a new window on ocean CO_2 uptake. *Global Biogeochemical Cycles* **7,** 353–368.

Trudinger C.M., Enting I.G., Francey R.J., Etheridge D.M. & Rayner P.J. (1999) Long-term variability in the global carbon cycle inferred from a high-precision CO_2 and $\delta^{13}C$ ice-core record. *Tellus B* **51,** 233–248.

Wang Y.P. & Leuning R. (1998) A two-leaf model for canopy

conductance, photosynthesis and partitioning of available energy I: model description and comparison with a multi-layered model. *Agricultural and Forest Meteorology* **91,** 89–111.

Wingate L., Seibt U., Moncrieff J.B., Javis P.G. & Lloyd J. (2007) Variations in ^{13}C discrimination during CO_2 exchange by *Picea sitchensis* branches in the field. *Plant, Cell & Environment* **30,** 600–616.

Winslow J.C., Hunt E.R., Jr. & Piper S.C. (2001) A globally applicable model of daily solar irradiance estimated from air temperature and precipitation data. *Ecological Modelling* **143,** 227–243.

Yakir D. & Wang X.F. (1996) Fluxes of CO_2 and water between terrestrial vegetation and the atmosphere estimated from isotope measurements. *Nature* **380,** 515–517.

Zhang J., Griffis T.J. & Baker J.M. (2006) Using continuous stable isotope measurements to partition net ecosystem CO_2 exchange into photosynthesis and respiration of a corn–soybean rotation ecosystem. *Plant, Cell & Environment* **29,** 483–496.

Zierl B. (2001) A water balance model to simulate drought in forested ecosystems and its application to the entire forested area in Switzerland. *Journal of Hydrology* **242,** 115–136.

Received 18 October 2006; received in revised form 12 February 2006; accepted for publication 29 May 2007

APPENDIX

Appendix A: sensitivity of stomatal conductance to soil water variability

The Parameter describing the sensitivity of stomatal conductance to soil water variability, f_w in Eqn 4 is a bulk water availability factor. It can be integrated from each layer's $f_{w,i}$ with a weighting factor w_i,

$$f_w = \sum_{i=1}^{n} f_{w,i} w_i, \tag{A1}$$

where n is the number of soil layers which contain roots. $f_{w,i}$ is a combined effect of soil water suction (ψ) and temperature ($T_{s,i}$), and it can be described as

$$f_{w,i} = 1/(f_i(\psi_i) f_i(T_{s,i})), \tag{A2}$$

where $f_i(\psi)$ and $f_i(T_{s,i})$ are calculated following Zierl (2001) and Bonan (1991), respectively:

$$f_i(\psi_i) = \begin{cases} 1 + ((\psi_i/10 - 1))^{\alpha} & \psi_i > 10\,m \\ 1 & \text{else} \end{cases}, \tag{A3}$$

$$f_i(T_{s,i}) = \begin{cases} \dfrac{1}{1 - \exp(t_1 T_{s,i}^{t_2})} & T_{s,i} > 0°C \\ \infty & \text{else} \end{cases}, \tag{A4}$$

where α, $T_{s,1}$ and $T_{s,2}$ are empirical parameters and equal to 0.8, –0.04 and 2.0, respectively.

The weighting factor w_i in Eqn A1 is calculated as

$$w_i = \frac{r_i f_{w,i}}{\sum_{i=1}^{n} r_i f_{w,i}}, \tag{A5}$$

where r_i is the root fraction in layer i.

Appendix B: isotopic signature of respired CO_2

The isotopic signature of respired CO_2 from different parts (from different pant organs or from dead organic matter in soil) is crucial for modeling isoflux. The monthly mean carbon isotopic signatures of respiration ($\delta^{13}C_R$) were interpolated on the basis of the discrete values calculated from all the night-time data in the campaigns (1998 through 2000) using Keeling-plot (Table B1). At first model test run, monthly $\delta^{13}C_R$ is approximated as the values of $\delta^{13}C_R^h$ (the isotopic signature of heterotrophic respiration (R_h) and $\delta^{13}C_R^a$ (the isotopic signature of autotrophic respiration (excluding foliar respiration if daytime). Once we gain the primary results, the monthly mean value of carbon isotopic signature of new fixed carbon $\overline{\delta^{13}C_{plant}}$ (Table B1) during growing season, can be calculated

$$\overline{\delta^{13}C_{plant}} = \overline{\delta^{13}C_a} - \overline{\Delta_{canopy}} \tag{B1}$$

Whereas for the non-growing season, $\overline{\delta^{13}C_{plant}}$ can be calculated using Eqn B1 by replacing monthly mean $\overline{\Delta_{canopy}}$ with its annual mean value.

It was formerly assumed (Fung *et al.* 1997) that overall autotrophic respiration ($\overline{\delta^{13}C_R^a}$) releases carbon of the same signature as gross photosynthetic products ($\overline{\delta^{13}C_{plant}}$). Accumulated investigations showed that in general this is not the case in real plants. Badeck *et al.* (2005) compiled evidence for widespread

Table B1. Monthly mean carbon isotopic signatures of respiration ($\overline{\delta^{13}C_R}$) and of new fixed carbon ($\overline{\delta^{13}C_{plant}}$) for model inputs[a]

Month	1	2	3	4	5	6	7	8	9	10	11	12
$\overline{\delta^{13}C_R}$ (‰)	–27.73	–27.73	–27.73	–27.73	–26.95	–26.17	–26.00	–26.34	–26.40	–26.07	–27.73	–27.73
$\overline{\delta^{13}C_{plant}}$ (‰)	–27.86	–27.93	–27.83	–27.85	–26.86	–26.98	–28.64	–27.89	–28.53	–26.77	–27.87	–27.98

[a] $\overline{\delta^{13}C_R}$ was interpolated on the basis of the discrete values calculated from all the night-time data in the campaigns (1998 through 2000) using Keeling-plot; whereas $\overline{\delta^{13}C_{plant}}$ was calculated by model test run (see Appendix B). For mode parameterization: $\overline{\delta^{13}C_R^h} \approx \overline{\delta^{13}C_R}$; $\overline{\delta^{13}C_{leaf}} \approx \overline{\delta^{13}C_{plant}}$; $\overline{\delta^{13}C_{stem}} \approx \overline{\delta^{13}C_{plant}} + 0.75‰$; and $\overline{\delta^{13}C_{root}} \approx \overline{\delta^{13}C_{plant}} + 1.5‰$.

post-photosynthetic fractionation that further modifies the isotopic signatures of individual plant organs and consequently leads to consistent differences in δ^{13}C between plant organs. Leaves are more depleted than roots and woody stems. In the updated VDS–BEPS–EASS isotope model, the respiratory flux from leaves during night-time is assumed to carry the signature of gross photosynthetic products (i.e. $\delta^{13}C_{leaf} = \overline{\delta^{13}C_{plant}}$). According to Badeck *et al.* (2005), the signatures of respiratory flux from woody stems ($\delta^{13}C_{stem}$) and roots ($\delta^{13}C_{root}$) are approximated as 0.75 and 1.5‰ less depleted than $\overline{\delta^{13}C_{plant}}$, respectively. For the final model run, the last term of Eqn 10 is calculated separately for individual plant organs,

$$\delta^{13}C_R^a R_a = \delta^{13}C_{leaf} R_{leaf} + \delta^{13}C_{stem} R_{stem} + \delta^{13}C_{root} R_{root}, \quad \text{(B2)}$$

where R_{leaf} is only available during night-time.